



Preparation and Study of Undoped and Al-Doped on the Structure and the Optical Properties of In_2S_3 Thin Film

Dhuha M. Abdullah¹   and Bushra H. Hussein^{2*}  

^{1,2}Department of Physics, College of Education for Pure Science (Ibn Al-Haitham), University of Baghdad, Baghdad, Iraq

*Corresponding Author.

Received: 17 January 2025

Accepted: 23 April 2025

Published: 20 July 2025

doi.org/10.30526/38.3.4110

Abstract

Undoped and aluminum-doped In_2S_3 chalcopyrite semiconductor thin films are deposited on glass substrates using the thermal evaporation process under a vacuum of 1.6×10^{-5} mbar, achieving a thickness of 500 nm. This study examines the impact of varying Al ratios of 0.0, 0.02 and 0.04 on properties of Al-doped In_2S_3 thin film. The structural characteristics of In_2S_3 thin films were studied by X-ray diffraction (XRD) and atomic force microscopy (AFM), revealing that the In_2S_3 film exhibits a polycrystalline structure and stable tetragonal β - In_2S_3 , with a preferred orientation of (109) at $2\theta = 27.3$. Furthermore, AFM is examining the exterior morphology of the film, revealing that both surface roughness and average diameter escalate with higher Al ratios, hence augmenting the crystallite size of the thin films. The UV/Vis spectrophotometer analyzed the optical properties of In_2S_3 films, revealing a maximum absorbance of 90% in the visible spectrum and a minimum transmittance. The films exhibited a bandgap that decreased by 0.04 for each ratio of Al, ultimately reaching a minimum value of Semiconductors In_2S_3 possess straight band gaps of 2.05, 1.98, and 1.95 eV, respectively. The computed optical constant encompasses the refractive index and the extinction coefficient. Real and imaginary components of the dielectric constant.

Keywords: Chalcopyrite semiconductors, n- In_2S_3 , Al Doped Thin film, XRD, AFM, Band gaps In_2S_3 , Thin film.

1. Introduction

Indium sulfide (In_2S_3) is a chemical compound represented by the formula In_2S_3 , distinguished as a red powder with a purity of 99.999%. It is an n-type binary semiconductor recognized for its significant optical transparency within the visible light spectrum (1).

Indium Sulphide (In_2S_3), a prominent member of the group III-V chalcogenide semiconductors, is a leading candidate for optoelectronic applications due to its exceptional characteristics, including strong photosensitivity, significant absorption coefficient, appropriate bandgap, low toxicity, and stability. Recently, In_2S_3 has attracted considerable interest owing to its distinctive features and its efficacy as an optical window material in photovoltaic solar cells. It is eco-friendly and non-toxic, rendering it a safer and more



sustainable substitute for conventional materials like cadmium sulfide (CdS) (2,3). Indium sulfide exhibits three polymorphic phases (α , β , γ), with the beta phase being the most stable and predominantly employed in thin-film applications. This phase demonstrates a lattice parameter of ($a = 7.619 \text{ \AA}$) and ($c = 32.329 \text{ \AA}$), contingent upon temperature at atmospheric pressure (4,5).

The qualities of In_2S_3 , along with its ecologically benign properties, make it a versatile material that may be produced by numerous procedures for diverse applications (6). In_2S_3 exhibits a broad bandgap of 2.0 to 2.9 eV, which can be adjusted by altering the material composition or via doping (7). It functions as a principal optical window material in solar cells for photovoltaic applications and is utilized as an active element to improve the efficacy of semiconductor batteries. Moreover, In_2S_3 is employed in photoelectrochemical cell applications that necessitate heightened sensitivity to light energy (8).

Prior scientific investigations have thoroughly examined the characteristics of In_2S_3 , especially when applied as thin films. These films have been produced with modern processes, including such as chemical bath deposition (3,9), vacuum thermal evaporation (10), spray pyrolysis (11), ultrasonic dispersion, physical vapor deposition (12), sputtering (13), electrodeposition (14), atomic layer deposition (ALD) (15), n-type semiconductor indium sulfide (In_2S_3) (5,16). This study studies the impact of Al doping ratio on the optical, XRD, AFM, and the relationship between these parameters, both with and without aluminum doping. The results collected are detailed and discussed below.

2. Materials and Methods

This study utilized In_2S_3 in the form of a red powder with a purity of 99.99% and stoichiometric weight ratios (2:3), Aluminum powder (Al) was employed as a dopant at concentrations of 0%, 2%, and 4% to modify In_2S_3 . Generally, there exists a threshold for the quantity of dopant that can be introduced without jeopardizing the material's characteristics. X-ray diffraction (XRD) analysis employing Cu-K radiation 1.5418 \AA was performed on a Malvern Panalytical Aeris system (UK) to describe the structural properties of In_2S_3 powder and thin film. The surface morphology of materials was examined utilizing atomic force microscopy (AFM; Flex AFM, Switzerland). The investigations indicated that the films exhibit a distinct crystalline structure. The crystalline dimensions were determined using the Scherrer equation, yielding accurate insights into the material's structural features (17, 18).

$$C.S = \frac{0.9\lambda}{\beta \cos\theta} \quad (1)$$

The symbol β represents the (FWHM) full widths at half maximum of the diffraction peak, which is a measure of the peak's broadening. The size of the crystallite (C.S.) can be determined using this parameter along with the Bragg angle (θ), which corresponds to the diffraction peak position. The lattice constants a and c for the tetragonal structure are determined using the following equation (19):

$$\frac{4\sin^2\theta}{\lambda^2} = \frac{h^2+k^2}{a^2} + \frac{l^2}{c^2} \quad (2)$$

The microstrain (ϵ) for the fabricated thin films from calculated using the following equation:

$$\epsilon = \frac{\beta \cos\theta}{4} \quad (3)$$

The dislocation density (δ) is the ratio of the lengths of the dislocation line to the volumes of the crystal. This can be calculated by the following (20):

$$\delta = \frac{1}{(C.S)^2} \quad (4)$$

Optical transmittance of thin film was measured across the wavelength ranges of 300–1100 nm to ascertain the energy bandgap (E_g). The transmittance and absorption spectra in this spectral range were examined, yielding insights into the optical properties of the produced film. Direct energy bandgap (E_g) was determined from the absorption spectra, utilizing Lambert's law and Tauc's equations. This relationship delineates the correlation between the absorption coefficient (α) and the photon energy ($h\nu$) as articulated by the subsequent equation (21, 22):

$$\alpha = 2.303 \frac{A}{t} \quad (5)$$

$$\alpha h\nu = D (h\nu - E_g)^r \quad (6)$$

Exact value of temperature-dependent constant D. The absorption coefficient is represented by the letter α , the energy of the incident photons is $h\nu$, and r is a parameter that indicates the type of optical transition. Absorption (A) and thickness (t). The subsequent relationships can be employed to compute optical constants, encompassing the extinction coefficient k , the refractive index n , and the real component ϵ_r , the imaginary parts ϵ_i of the dielectric constant, and the reflection R (23-25):

$$k = \frac{\alpha \lambda}{4\pi} \quad (7)$$

$$n = \left[\frac{4R}{(1-R)^2} - k^2 \right]^{1/2} - \frac{(1+R)}{(1-R)} \quad (8)$$

$$\epsilon_i = 2nk \quad (9)$$

$$\epsilon_r = n^2 - k^2 \quad (10)$$

3. Results and Discussion

The incorporation of aluminum (Al) into In_2S_3 thin films is a substantial advancement in improving their crystallographic and physical characteristics. **Figure (1)** displays the XRD pattern for In_2S_3 thin film with (Al = 0.0, 0.02, and 0.04) at RT and a thickness of 500 nanometers. This Figure shows that the In_2S_3 thin films have a polycrystalline stable tetragonal $\beta\text{-In}_2\text{S}_3$, with (109) preferred orientation at $2\theta \approx 27.3$, and this agrees with the study (26). **Figure (1)** illustrates that the crystalline peaks in the XRD patterns display minor shifts with aluminum incorporation, signifying its effect on the lattice strain inside the crystal structure. This phenomenon is ascribed to the replacement of aluminum atoms at designated lattice positions within the In_2S_3 crystal. **Table (1)** indicates that the measured diffraction angles and interplanar spacings align well with the standard values documented in the ICDD card (00-025-0390). This alignment verifies that the addition of aluminum does not adversely affect the phase stability of the In_2S_3 crystal structure. The incorporation of aluminum diminished the full widths at half maximum of the diffraction peaks, indicating an enhancement in crystallite size. This enhancement is ascribed to the diminished crystal strain and improved homogeneity in the crystalline structure and the values of lattice constants $a=7.619 \text{ \AA}$ and $c=32.329 \text{ \AA}$ is very close to researches (16). Aluminum also facilitated a reduction in crystal strain (ϵ) and dislocation density (δ), indicating enhanced crystalline quality. The alleviation of strain further improves the structural efficacy of the thin films.

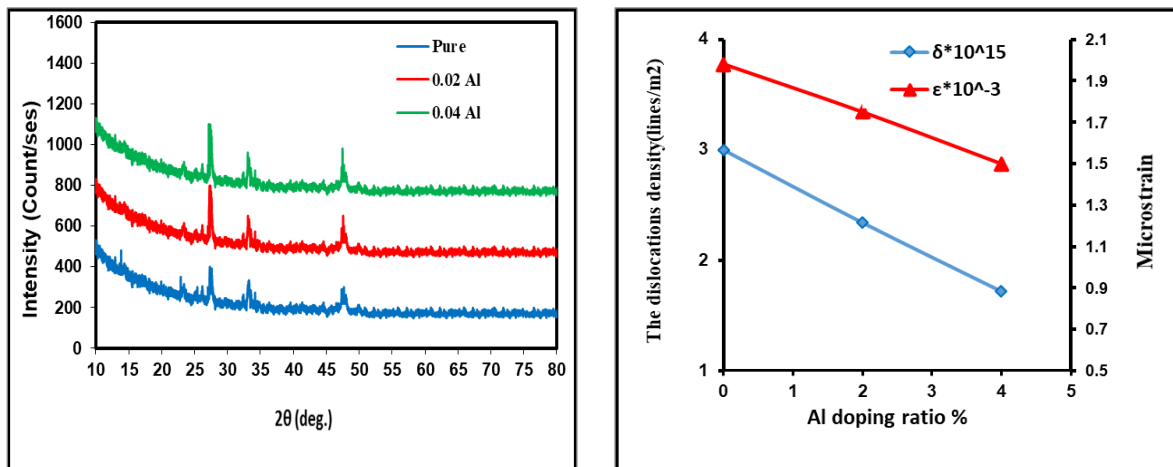


Figure 1. XRD patterns of In₂S₃ and In₂S₃ doped with (0.0, 0.02, 0.04) Al.

Table 1. X-ray diffraction data from experiments for In₂S₃ thin film at Al 0.0, 0.02, and 0.04.

Al ratio	$d_{exp.}$ deg.	$2\theta_{exp.}$ deg.	(hkl)	FWHM deg.	C.S nm	$\delta \cdot 10^{15}$ lines/m ²	$\epsilon \cdot 10^{-3}$
In ₂ S ₃ (Al = 0.0)	3.262847	27.3	(109)	0.4674	18.2703	2.9958	1.98
	2.695323	33.199	(0012)				
	1.905073	47.68	(2212)				
In ₂ S ₃ (Al = 0.02)	3.274615	27.2	(109)	0.4131	20.66747	2.3411	1.75
	2.703158	33.1	(0012)				
	1.908088	47.6	(2212)				
In ₂ S ₃ (Al = 0.04)	3.281719	27.14	(109)	0.3541	24.10803	1.7206	1.5
	2.705542	33.07	(0012)				
	1.913162	47.466	(2212)				

The computations for micro-strain & dislocation density have been completed and are displayed in **Table (1)**. Reduction in micro strain and dislocation density becomes evident with rising Aluminum ratios. The observed phenomena are due to a positive association between the strain of micro and the full widths at half maximum (FWHM) of the principal peak, with a negative correlation between dislocation density and crystallite size. The noted decrease in defects in In₂S₃ (Al = 0.0, 0.02, and 0.04) thin films with rising Aluminum ratios indicates an improvement in their crystalline structure.

The examination of atomic force microscopy (AFM) data for In₂S₃ thin films doped with different aluminum (Al) concentrations uncovers significant insights into the influence of aluminum on surface structure and characteristics. **Figure (2)** and **Table (2)** illustrate that an increase in aluminum content within the thin films led to a significant elevation in surface roughness relative to undoped films. This behavior demonstrates that aluminum significantly alters the surface structure of the material. These alterations augment the interaction between the surface and the ambient environment, consequently enhancing the optical and electrical properties of the material. The augmentation of aluminum concentration resulted in an elevation of the root mean square (RMS) roughness and grain size. This impact underscores aluminum's influence on modifying the crystallization pattern and grain distribution, hence enhancing the material's physical qualities.

These structural modifications indicate the development of more consistent nanoscale architectures, which boost material performance across many technical applications. The In₂S₃ sample (Al = 0.04) exhibits a significant magnitude. This tendency can be attributed to enhanced atomic mobility, resulting in the aggregation of particles, especially bigger ones.

This aggregation finally signifies an enhancement in the texture of the films. These observations validate the XRD results.

Table 2. AFM data for In₂S₃ thin film doped (0.0, 0.02, 0.04) Al.

Thickness (500 nm)	Average diameter nm	Roughness average nm	Root means square
In ₂ S ₃ (Al = 0.0)	39.28	3.969	6.005
In ₂ S ₃ (Al = 0.02)	47.69	11.01	21.84
In ₂ S ₃ (Al = 0.04)	48.57	21.36	35.34

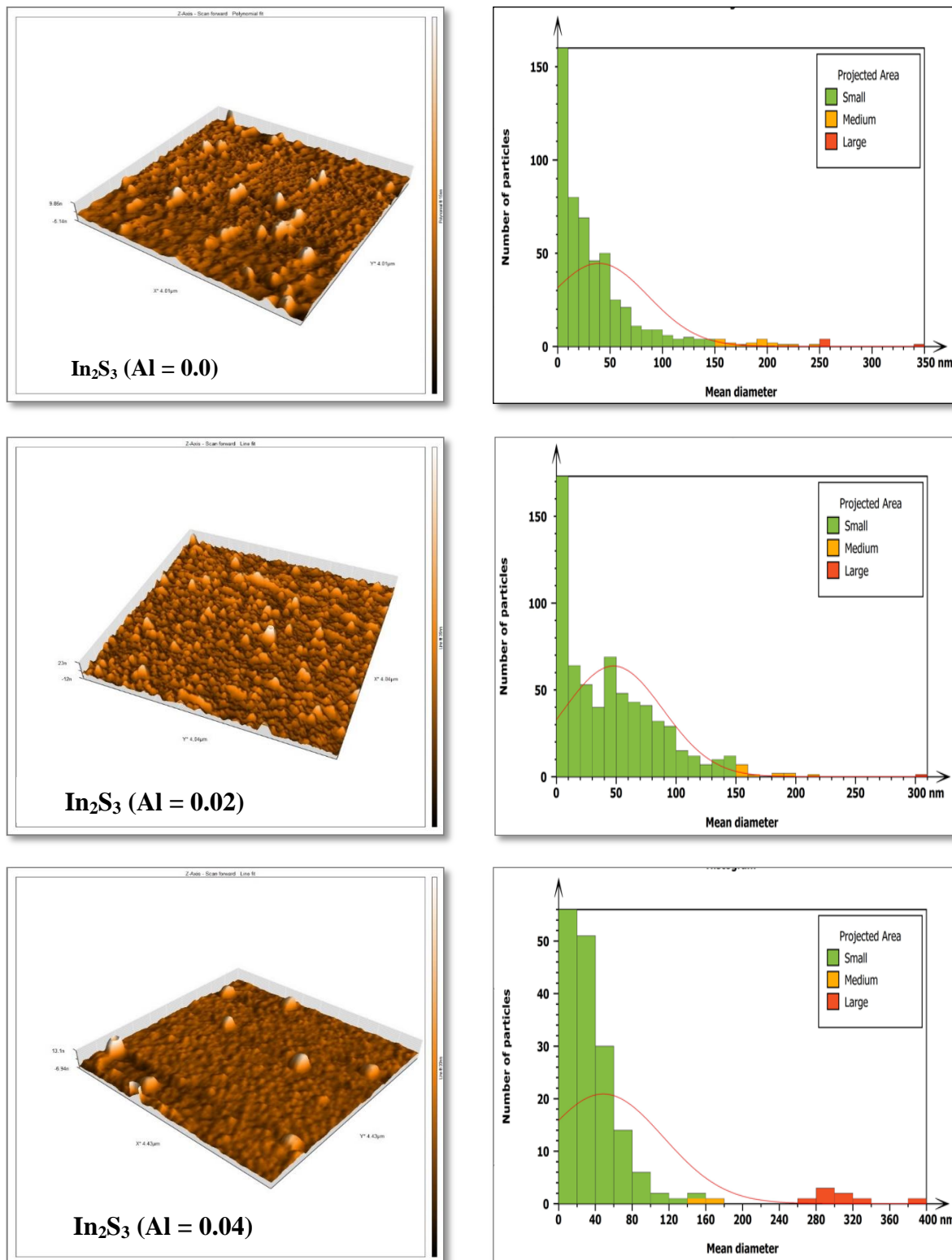


Figure 2. AFM images of undoped In₂S₃(0.0) and In₂S₃ doped with (0.02, 0.04) Al.

Based on the absorbance and transmittance values throughout the range of 300-1100 nm, the transmittance relationship is illustrated according to the wavelength shown in **Figure (3)**, indicating the findings for In₂S₃ (0.0) and In₂S₃ doped with (0.02, 0.04). All films exhibit a high absorbance rate of approximately 90% in the 300-550 nm spectral range. When doped with 0.02 and 0.04 Al, a decrease in transmittance values is observed, accompanied by an increase in absorbance and a shift of the fundamental absorption edge toward longer wavelengths (lower energy). This behavior can be ascribed to the use of X-ray diffraction (XRD) and atomic force microscopy data to know the correlations between surface morphology and observed increase in absorbance (27, 28). This indicates that after adding the Al procedure, the absorbance value of these thin films demonstrates an increasing tendency. This rise is due to the absorption of photons by free carriers, resulting in a decrease in transmittance. Alternatively, it may be associated with the evolution of crystallite dimensions (29,30). Therefore, the capacity to absorb low-energy photons is feasible.

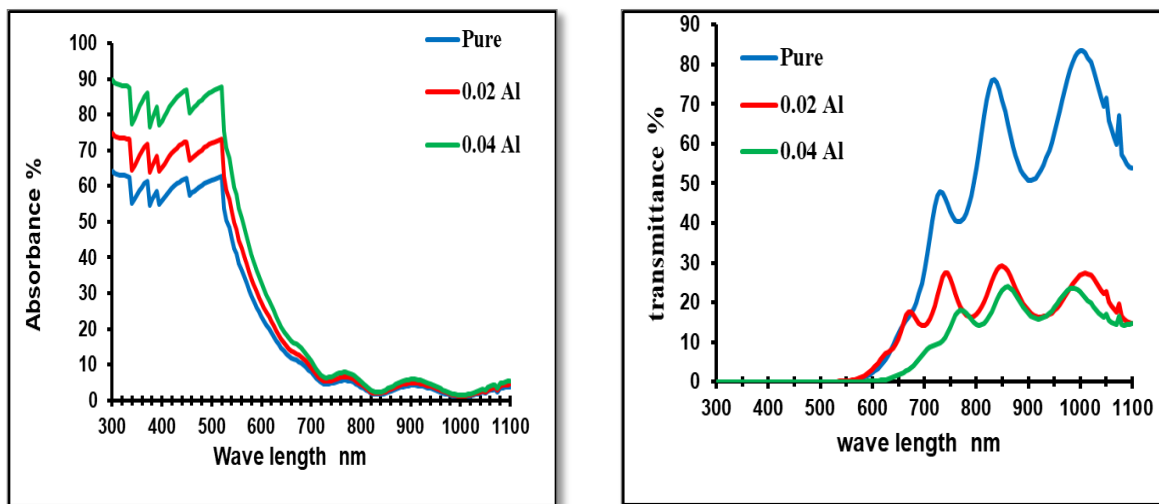


Figure 3. The transmittance and absorption spectrum of In₂S₃ doped with (0.02, 0.04) Al.

Figure (4) illustrates the variations of the absorption coefficient as a function. For In₂S₃ (0.0) and In₂S₃ doped with (0.02, 0.04) Al, we observe a gradual increase in the absorption coefficient with rising photon energy. This pronounced increase facilitates the determination of the fundamental absorption edge. The results indicate that elevating the addition of Al significantly enhances the absorption coefficient values, particularly at lower energies. **Figure (4)** indicates this. As the absorption edge approaches, the fundamentals shift towards lower photon energy. The absorption coefficient for all instances exceeds 10⁴ in the high energy range, signifying direct electronic transfers, consistent with the findings of research (3). The energy gap was ascertained utilizing the Tauc equations. **Figure (4)** illustrates the variation of E_g In₂S₃ (0.0) and In₂S₃ doped with (0.02, 0.04) Al. The transition of the In₂S₃ film was calculated to be directly permitted, ranging from 2.05 eV to 1.95 eV, in strong agreement with (1,16).

Table 3. Optical factors (E_g^{opt}, α, n, k, ε_r & ε_i) In₂S₃ with (doped with (0.02, 0.04) Al where (Cutoff wavelength)λ = 520 nm.

Thickness (500 nm)	E _g ^{opt} (eV)	α × 10 ⁴ (cm ⁻¹)	n	K	ε _r	ε _i
In ₂ S ₃ (Al = 0.0)	2.05	2.88	2.57	0.119	6.59	0.614
In ₂ S ₃ (Al = 0.02)	1.98	3.36	2.07	0.139	4.29	0.579
In ₂ S ₃ (Al = 0.04)	1.95	4.04	1.566	0.167	2.43	0.44

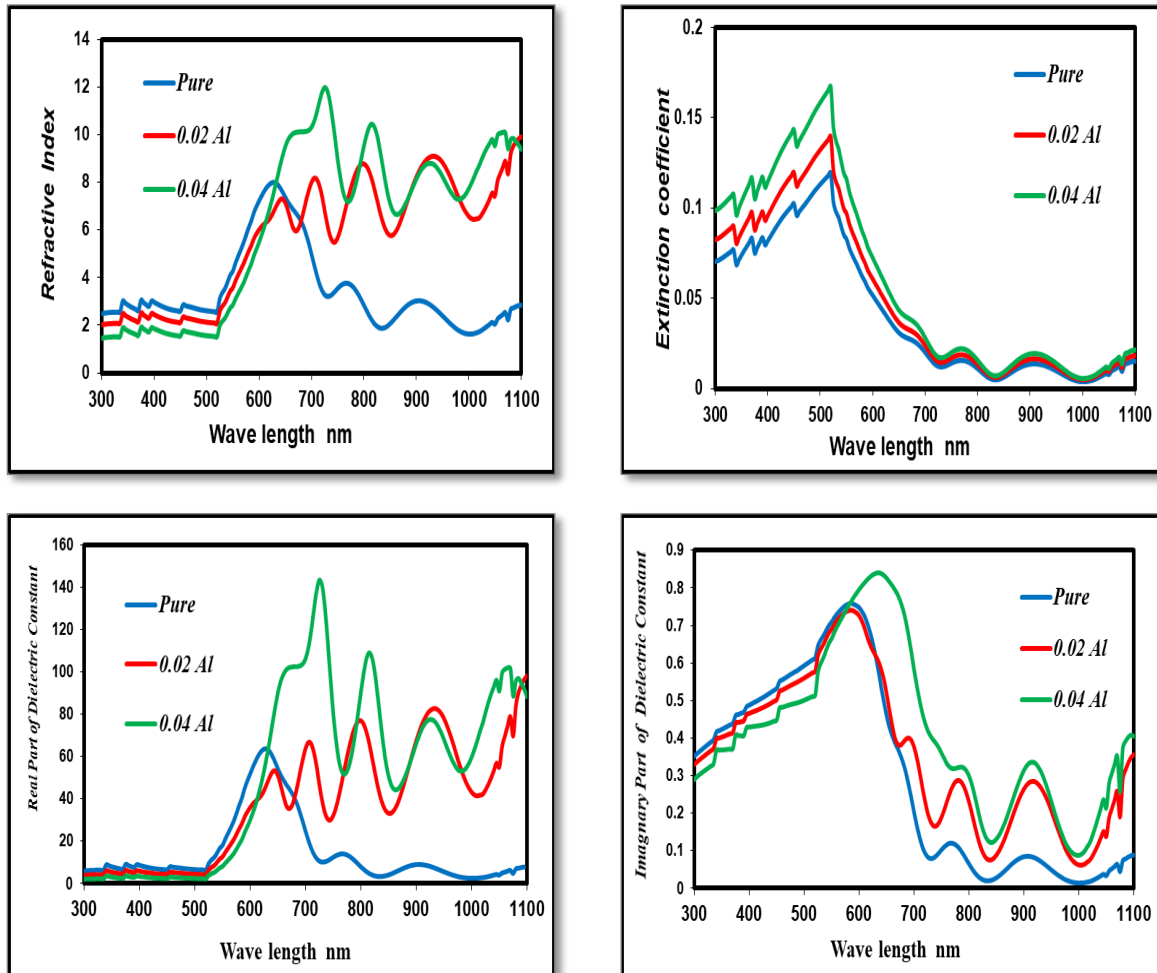


Figure 4. The fluctuation in the optical factors (refractive index, Extinction coefficient, and real & imaginary components for dielectric constants) with wavelength of In_2S_3 doped with (0.02, 0.04) Al.

The extinction coefficient was determined based on the calculated absorption coefficients using relationship (7). The attenuation of electromagnetic radiation intensity signifies the energy absorbed by the thin layers. The extinction coefficient demonstrates a gradual increase with rising photon energy, followed by a sharp increase at elevated photon energies, indicating enhanced absorption, which subsequently results in an increased absorption coefficient at the Al doping ratio. The curves consistently exhibit similar behavior as previously described, with the absorption edge shifting towards lower photon energies, so confirming that the Al doping ratio significantly enhances the extinction coefficient (31). **Figure (4)** illustrates the variation of refractive index with the wavelengths of In_2S_3 doped with (0.02, 0.04) aluminum film. The refractive index curve closely mirrors the characteristics of reflection. According to the link about the refractive index and reflection, **Table (3)** presents the refractive index values for all films at a constant wavelength of 520 nm (within the visible spectrum). The decline in n values during doping with Al is due to the decrease in corresponding reflections caused by structural and compositional alterations that transpire during the doping process. This discovery aligns with prior research (1). The correlation between the real (ϵ_r) and imaginary (ϵ_i) components of the dielectric constants is affected by the values of n and k . At a wavelength of 520 nm, the values of ϵ_r and ϵ_i diminish due to the analogous behavior between ϵ_r and n ; the behavior of ϵ_i closely mirrors that of k , which is mostly contingent upon the k value. The value of ϵ_i is less than that of the thin film, signifying minimal dielectric loss. The best optical aluminum doping ratio was observed at 0.04.

4. Conclusion

This research yielded numerous conclusions: The potential for In₂S₃ films with the thermal evaporation technique yields polycrystalline films, and an increase in Al doping ratio leads to little shifts in the diffraction spectrum towards higher angles. All films exhibited allowed direct electronic transitions, with the energy gap diminishing as the Al doping ratio increased. The evaluation of all films revealed an energy range of 2.05-1.95 eV, signifying their potential for junction formation in solar cells. An increase in the Al doping ratio resulted in a shift of the transmittance and absorption peak towards lower photon energies, indicating enhanced absorbance. The extinction coefficient rises as a result of an elevated absorption coefficient.

Acknowledgment

Authors thank the Thin Film Lab., Department of Physics, College of Education for Pure Science /Ibn Al-Haitham, University of Baghdad.

Conflict of Interest

Conflict of Interest. The authors declare that they have no conflicts of interest.

Funding

We hereby confirm that all the Figures and Tables in the manuscript are ours.

Ethical Clearance

The project was approved by the local ethical committee at the University of Baghdad

References

1. Alamoudi E, Timoumi A, Parida P, Ganguli B. [The synthesis and the effect of Cu on optoelectronic qualities of \$\beta\$ -In₂S₃ as a window layer for CIGS thin film solar cells](https://doi.org/10.1016/j.rinp.2022.105858). Results Phys. 2022;40: 105858. <https://doi.org/10.1016/j.rinp.2022.105858>
2. Mohd Sh, Altowyan AS, Maiz F, Hakami J. Influence of incorporation of samarium (Sm³⁺) on the structural and optoelectronic properties of In₂S₃ thin film for photodetector applications. J. Photochem. Photobiol. A Chem. 2023; 441: 114736. <https://doi.org/10.1016/j.jphotochem.2023.114736>
3. Rodríguez-Hernández PE, Quiñones-Galván JG, Marasamy L, Morales-Luna M, Santos-Cruz J, Arias-Cerón JS, Zelaya-Angel O, de Moure-Flores F. Optoelectronic properties of undoped and Al, B and Ga-doped In₂S₃ thin films grown by CBD on flexible PET/ITO substrates, J. Mater. Sci. Sem. Prog. 2019 ;103(15): 104600, <https://doi.org/10.1016/j.mssp.2019.104600>
4. Alagarasan D, Hegde SS, Naik R, Murahari P, Shetty HD, Alkallas FH, Ben A, Trabelsi G, Khan FS, AlFaify S, Shkir M. Fabrication of Bi-doped In₂S₃ thin films for highly sensitive UV photodetector applications, Journal of Photochemistry and Photobiology. 2024 ; 454 : 115697. <https://www.sciencedirect.com/science/article/abs/pii/S1010603024002417>
5. Atre PP, Desai MA, Vyas Akshay N, Sartale SD, Pawar BN. Deposition of β -In₂S₃ Photosensitive Thin Films by Ultrasonic Spray Pyrolysis, Journal of ES Energy and Environment, 2021; 12: 52-59. <https://www.espublisher.com/journals/articledetails/403/>
6. Hsiao, YJ, Lu CH, Ji LW, Meen TH, Chen YL, Chi HP. Characterization of photovoltaics with In₂S₃ nanoflakes/p-Si heterojunction. Nanoscale Res. Lett. 2014; 9(32): 1-7. <https://link.springer.com/article/10.1186/1556-276X-9-32>
7. Thierno S, Bouchaib H, Bernabe M, Mollar M, Larbi L, Mounir F. Elaboration and characterization of In₂S₃ thin films by spray pyrolysis with [S]/[In]=3 ratio. IEEE 2013; 978: 1-4673-6374. <https://ieeexplore.ieee.org/document/6529664>

8. Pulipaka S, Koushik AKS, Deepa M, Meduri P. Enhanced photoelectrochemical activity of Co-doped β -In₂S₃ nanoflakes as photoanodes for water splitting. RSC Adv. 2019; 9(3): 1335–1340. <https://pubmed.ncbi.nlm.nih.gov/35518026/>
9. Rodriguez-Hernandez PE, Moure-Flores FDE, Guillen Cervantes A, Campos-Gonzalez E, Santos-Cruz J, Mayen-Hernandez SA, Arias-Ceron JS, Olvera MDelal, Zelaya-Ángel O, Contreras-Puented G. Physical Properties Of In₂S₃ Thin Films Grown By Chemical Bath Deposition At Different Temperatures. Chal. Lett. 2016; 13(8): 389 – 396. https://www.chalcogen.ro/389_RodriguezPE.pdf
10. Rasool S, Saritha K, Ramakrishna Reddy KT, Ramakrishna Reddy K, Bychto L, Patryn A, Maliński M, Tivanov MS, Gremenok VF. Optical properties of thermally evaporated In₂S₃ thin films measured using photoacoustic spectroscopy. Materials Science in Semiconductor Processing 2017; 4-8. <http://dx.doi.org/10.1016/j.mssp.2017.09.009>
11. Souissi R, Bouguila N, Bendahan M, Fiorido T, Aguir K, Kraini M, Vázquez-Vázquez C, Labidi A. Highly sensitive nitrogen dioxide gas sensors based on sprayed β -In₂S₃ film. Sensors and Actuators B: Chemical. 2020;319(15): 128280. <https://doi.org/10.1016/j.snb.2020.128280>
12. Kraini M, Bouguila N, El Ghouli J. Nickel doping effect on properties of sprayed In₂S₃ films. Indian J Phys 2018;92(8):989–997. <https://link.springer.com/article/10.1007/s12648-018-1195-3>
13. Karthikeyan S, Hill AE, Pilkington RD. Low temperature pulsed direct current magnetron sputtering technique for single phase β -In₂S₃ buffer layers for solar cell applications. Applied Surface Science, 2017;418:199-206 <https://colab.ws/articles/10.1016%2Fj.apsusc.2017.01.147>
14. Mughal MA, Alqudsi A, Rao PM, Masroor M, Ichwani R, Zhou L, Giri B, All-electrodeposited p-Cu₂ZnSnS₄/n-In₂S₃ Heterojunction Formation for Solar Cell Applications. IEEE. 2018; 142-147. <https://10.1109/PVSC.2018.8548079>
15. Sterner J, Malmström J, Stolt L. Study on ALD In₂S₃/Cu (In, Ga) Se₂ interface formation. Progress in Photovoltaics: Research and Applications. 2005; 13(3):179-193. <https://onlinelibrary.wiley.com/doi/abs/10.1002/pip.595>
16. Akcay N, Erenler B, Ozen Y, Gremenok V, Buskis KP, Ozcelik S. Effect of Post-thermal Annealing on the Structural, Morphological, and Optical Properties of RF-sputtered In₂S₃ Thin Films. Journal of Science. 2023; 36:1351-1367. <https://doi.org/10.35378/gujs.1075405>
17. Khudayer IH, Hussien BH. Study of Some Structural and Optical Properties of AgAlSe₂ Thin Films. Ibn AL-Haitham J Pure Appl Sci. 2017;29(2):41–51. <https://www.iasj.net/iasj/download/d06fb3c7d8db8a28>
18. Al-Maiyaly BKH. characterization of n-CdO: Mg/p-Si heterojunction dependence on annealing temperature. Ibn AL-Haitham J Pure Appl Sci. 2017;29(3):14–25. <https://jih.uobaghdad.Edu.iq/index.php/j/article/view/8>
19. Hübschen G, Altpeter I, Tschuncky R, Herrmann HG. Materials characterization using nondestructive evaluation (NDE) methods. 2nd ed. Woodhead publishing; 2016. ISBN: 9780081000571
20. Athab RH, Hussein BH. Fabrication and investigation of zinc telluride thin films. Chalcogenide Lett. 2023;20(7):477–85. <https://doi.org/10.15251/CL.2023.207.477>
21. Hussein BH, Khudayer IH, Mustafa MH, Shaban AH. Effect of V, In and Cu doping on properties of p-type ZnSe/Si heterojunction solar cell. Prog Ind Ecol An Int J. 2019;13(2):173–86. <https://doi.org/10.1504/PIE.2019.099358>
22. Hussein BH, Hassun HK. GROWTH AND OPTOELECTRONIC PROPERTIES OF p-CuO:Al/n-Si HETEROJUNCTION. J Ovonic Res. 2020;16(5):267–71. <https://chalcogen.ro/267-MaiyalyBKH.pdf>
23. Hussein BH, Hassun HK, Maiyaly BK, Aleabi SH. Effect of copper on physical properties of CdO thin films and n-CdO: Cu/p-Si heterojunction. J Ovonic Res. 2022;18:37–42. <https://doi.org/10.15251/JOR.2022.181.37>
24. Sze SM, Li Y, Ng KK. Physics of semiconductor devices. 3rd ed. John Wiley & sons; 2021. ISBN: 9780470068328, <https://doi.org/10.1002/0470068329>.

25. Schroder DK. Semiconductor material and device characterization. 3rd ed. John Wiley & Sons; 2015. ISBN:9780471749097, <https://doi.org/10.1002/0471749095>.
26. Akcay N, Erenler B, Ozen Y, Gremenok VF, Buskis KP and Ozcelik S. Effect of Post-thermal Annealing on the Structural, Morphological, and Optical Properties of RF-sputtered In₂S₃ Thin Films. Journal of Science. 2023; 36: 1351-1367. <https://doi.org/10.35378/gujs.1075405>
27. Kim K, Ahn SK, Choi JH, Yoo J, Eo YJ, Cho JS, et al. Highly efficient Ag-alloyed Cu (In, Ga) Se₂ solar cells with wide bandgaps and their application to chalcopyrite-based tandem solar cells. Nano Energy. 2018;48:345–52. <https://doi.org/10.1016/j.nanoen.2018.03.052>
28. Ahmed GS, Hussein BH, Hassun HK, Salman EMT, Athab RH. Fabrication and Improvement of Optoelectronic Properties of Copper Chalcogenide Thin Films. Iraqi J Appl Phys. 2023;19(4):223–8. <https://doi.www.iasj.net/iasj/article/284872>
29. Tigau N, Ciupina V, Prodan G, Rusu GI, Gheorghies C, Vasile E. The influence of heat treatment on the electrical conductivity of antimony trioxide thin films. J Optoelectron Adv Mater. 2003;5(4):907–12. https://doi.old.joam.inoe.ro/arhiva/pdf5_4/Tigau.pdf
30. Sobhi SN, Hussein BH. Study the Influence of Antimony Dopant and Annealing on Structural, Optical and Hall Parameters of AgInSe₂ Thin Film. Ibn AL-Haitham J Pure Appl Sci. 2022;35(3):16–24. <https://doi.org/10.30526/35.3.2824>
31. Athab RH, Hussein BH. Growth and Characterization of Vacuum Annealing AgCuInSe₂ Thin Film. Ibn AL-Haitham J Pure Appl Sci. 2022;35(4):45–54. <https://doi.org/10.30526/35.4.2868>